Farm vehicles approaching weights of sauropods exceed safe mechanical limits for soil functioning

Thomas Keller[a,b,1] and Dani Or[c,d]

Mechanization has greatly contributed to the success of modern agriculture, with vastly expanded food production capabilities achieved by the higher capacity of farm machinery. However, the increase in capacity has been accompanied by higher vehicle weights that increase risks of subsoil compaction. We show here that while surface contact stresses remained nearly constant over the course of modern mechanization, subsoil stresses have propagated into deeper soil layers and now exceed safe mechanical limits for soil ecological functioning. We developed a global map for delineating subsoil compaction susceptibility based on estimates of mechanization level, mean tractor size, soil texture, and climatic conditions. The alarming trend of chronic subsoil compaction risk over 20% of arable land, with potential loss of productivity, calls for a more stringent design of farm machinery that considers intrinsic subsoil mechanical limits. As the total weight of modern harvesters is now approaching that of the largest animals that walked Earth, the sauropods, a paradox emerges of potential prehistoric subsoil compaction. We hypothesize that unconstrained roaming of sauropods would have had similar adverse effects on land productivity as modern farm vehicles, suggesting that ecological strategies for reducing subsoil compaction, including fixed foraging trails, must have guided these prehistoric giants.

soil compaction | soil functions | crop productivity | mechanization | dinosaurs

Civilization relies on soil for provision of numerous ecosystem services (1, 2). Invariably, these services are predicated on maintenance of favorable conditions for soil fauna and flora (3, 4). Soil structure emerges as a central trait for many ecological, hydrological, and agronomical functions, serving as a fragile scaffolding for biological activity (5–7). The intensification of modern food production with its reliance on efficient agrotechnical practices presents a growing risk to the maintenance of favorable soil structure and poses a threat to the long-term productivity of arable land. Of particular concern is the steady increase in the weight of modern agricultural vehicles that may have already caused chronic subsoil compaction (8–11), with potential loss of soil productivity and functioning (12, 13). In contrast with well-known (and visible) effects of soil surface compaction, an insidious and largely overlooked threat is the gradual compaction of soil below the annual tillage depth, referred to as subsoil compaction. Evidence from long-term field studies shows that subsoil compaction is difficult to reverse and can impair soil functioning for years to decades (14, 15).

Here, we analyze historical trends in combine harvester weights and their associated agricultural tires to show that while soil surface stresses of farm vehicles remained nearly constant from the 1960s to date, the stresses in the subsoil, i.e., in the plant root zone, have steadily increased. Our analysis implies that the design of larger agricultural vehicles has been guided primarily by maintaining a constant contact area–weight relationships, similar to the evolutionary scaling relationship between footprint size and body mass of walking terrestrial animals. However, the limited consideration of stress propagation into the subsurface plant root zone has caused exceedance of soil mechanical limits in the subsoil that impairs soil ecological functioning. We present an index of subsoil compaction susceptibility, calculated as the ratio of estimated typical soil stress to soil strength at a 0.5-m depth. A global map of this index delineates regions where present mechanization levels are likely to exceed safe mechanical limits for soil functioning.

The evolutionary trend in contact area–mass scaling reveals a potential prehistorical paradox concerning the largest animals that walked Earth: sauropods. Evidence suggests that while their footprint size–body mass relationship follows a similar scaling law as for contemporary mammals and farm machinery, their body mass (or load per foot) exceeded that of the heaviest modern farm vehicles that are associated with inducing chronic root zone compaction. While resolving this prehistorical paradox is beyond the

Significance

Mechanization has transformed agriculture over the past century, greatly improving crop production efficiency. However, the higher capacity has resulted in increased farm vehicle weights. We show that while machinery design maintains constant surface contact stresses, an insidious and largely overlooked threat of subsoil compaction has developed. We demonstrate that modern vehicles induce high soil stresses that now exceed critical mechanical thresholds for many arable soils, inducing chronic soil compaction in root zones below tillage depths and adversely affecting soil functioning. We draw parallels between modern farm vehicles and the heaviest animals that walked Earth: sauropods. We hypothesize that these prehistoric giants may have induced subsoil compaction, thus presenting a paradox for productivity of the land that supported them.

Author affiliations: [a]Department of Soil & Environment, Swedish University of Agricultural Sciences, 75007 Uppsala, Sweden; [b]Department of Agroecology & Environment, Agroscope, 8046 Zürich, Switzerland; [c]Department of Environmental Systems Science, Swiss Federal Institute of Technology in Zürich, 8092 Zürich, Switzerland; and [d]Division of Hydrologic Sciences, Desert Research Institute, Reno, NV 89512

[1]To whom correspondence may be addressed. Email: thomas.keller@slu.se.

scope of the study, we argue that this putative mechanical limit on land productivity must have constrained the movement, foraging patterns, and habitats of these vegetarian giants.

Soil Mechanical Properties Constrain the Contact Area–Mass Relationship

The total weight of laden combine harvesters has increased nearly 10-fold, from around 4,000 kg in 1958 to about 36,000 kg in 2020 (*SI Appendix*, Table S1), with wheel loads of the front axle increasing from 1,500 to 12,500 kg (*SI Appendix, Table S1*). The rapid evolution in farm machinery weight has been driven by an increase in power and capacity with wider cutter boards and larger grain tank capacity (*SI Appendix*, Fig. S1), aimed at improving harvest efficiency. In the same time, the agricultural tires have become larger (i.e., more voluminous and wider; *SI Appendix*, Table S1) and more flexible, allowing lower tire inflation pressure at a given load (16). In other words, agricultural machinery designers have adjusted the tire–soil contact area to maintain nearly constant contact stresses (*SI Appendix*, Table S1). This reflects an important design criterion for adjusting average surface stresses to prevent sinking into the soil, thus ensuring floatation and traction.

Interestingly, similar principles have guided the evolution of footprint size of land animals (17, 18). For example, mammals follow unique scaling relationships between log contact area and log body mass (Fig. 1). Special adjustments are found for animals inhabiting regions with soft ground, such as camels that must float over sandy landscapes and thus have evolved with a relatively high footprint contact area. Our data (*SI Appendix*, Table S2) suggest that modern agricultural machinery belongs to the floating category, with a higher contact area relative to average mammal footprints. Arable soil is often soft due to annual tillage operations and due to high soil moisture conditions, especially in temperate regions. Another consideration for this design optimization is that tire sinking increases rolling resistance, power requirement, and fuel consumption (19). Notably, even the heaviest animals that walked the land, the prehistoric sauropods, seem to follow the floating category (Fig. 1). This suggests that across soil types and climatic conditions, a relatively narrow range of surface contact stresses (centered around 230 kPa; Figs. 1 and 2*A*) prevents
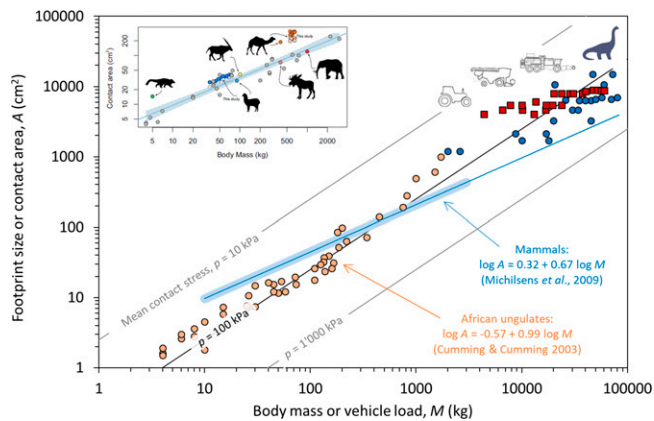

Fig. 1. Scaling relationship between footprint size (contact area) and body or vehicle mass. Blue circles represent sauropods (data in *SI Appendix*, Table S3), and red squares represent agricultural machinery, with tire characteristics given in *SI Appendix*, Table S2. The orange circles are from Cumming and Cumming (17), and the light blue line is the scaling law of Michilisens et al. (18), also presented in the inset taken from Clemente et al. (72). Note the relatively narrow range of surface contact stress that spans the entire range of animals (extant and extinct) and agricultural machinery.
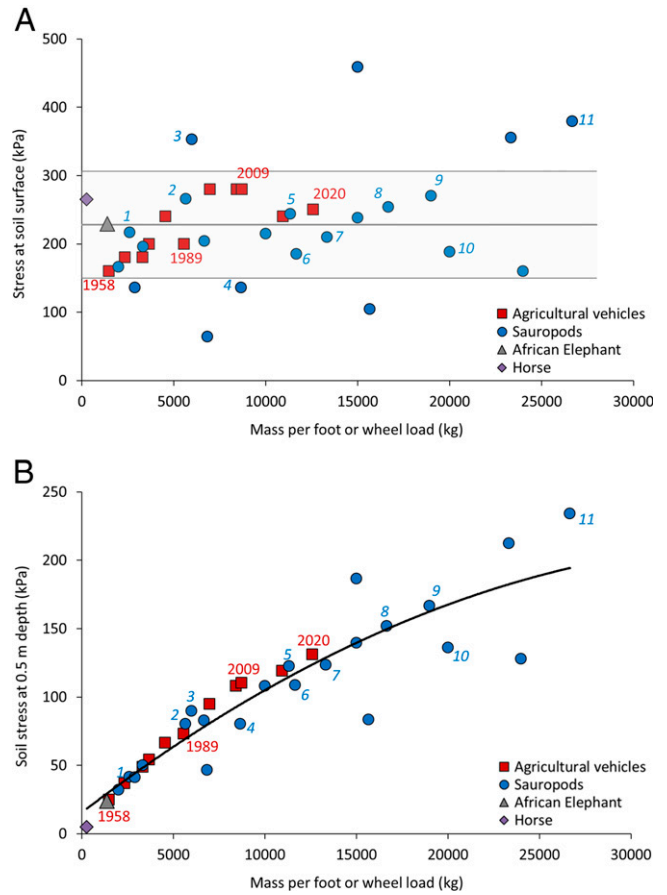

Fig. 2. Subsoil stress but not surface stress is affected by body or vehicle mass. (*A*) Surface stress and (*B*) soil stress at a 0.5-m depth as a function of mass per foot or wheel load. Bold black lines are trend lines, and the gray area in *A* indicates mean value ± SD. Numbers in red indicate the year of a typical combine harvester of that time, blue numbers in italics refer to sauropods (1, *Plateosaurus engelhardti*; 2, *Morosaurus agilis*; 3, *Cetiosaurus* sp.; 4, *Argyrosaurus superbus*; 5, *Prontopodus* sp.; 6, *Neosodon praecursor*; 7, *Sauropodichnus giganteus*; 8, *Brachiosaurus* sp.; 9, cf. *Prontopodus birdi*; 10, *Barosauros lentus*; 11, cf. *Argentinosaurus*).

sinking into soil. The analyses of Cumming and Cumming (17) demonstrate that hoof pressure is relatively constant irrespective of body size.

Exceedance of Critical Stresses in Subsoil

While surface contact stresses of agricultural vehicles have not changed much over the course of modern mechanization (Figs. 1 and 2*A*), we seek to emphasize an overlooked consequence of increased vehicle weight, namely, the increase in the magnitudes and penetration depths of subsoil stresses (Fig. 2*B*). With increasing depth, vehicle-applied soil stress becomes dependent primarily on wheel load and less affected by (surface) contact stress (Fig. 2) (20, 21). As demonstrated theoretically in *SI Appendix*, Fig. S2, and measured by, e.g., Smith and Dickson (22) and Horn and Fleige (23) for identical contact stress, higher wheel loads result in higher stress levels into the subsoil. Higher stresses that propagate into deeper and often wetter soil layers raise the prospects for subsoil compaction within sensitive crop root zones that lie below tillage depths. Experimental evidence from in situ measurements suggests a nearly constant critical limiting stress for internal soil deformation of about 50 kPa for moist soils in temperate regions (24). This threshold represents an estimate based on in situ measurements; however, local soil conditions can modify this value (texture, soil organic

carbon, soil structure, and soil moisture affect soil strength) (25). Using estimates of soil precompression stress as a critical stress (i.e., soil strength) threshold (*SI Appendix*, section 5 and Figs. S3 and S4), we show that subsoil stresses under farm vehicles have affected progressively deeper soil layers over the past six decades (Fig. 3). While soil compaction as indicated by exceedance of the critical stress threshold had been restricted to shallow soil layers within the annual tillage depth a few decades ago, it has now penetrated deeper into the subsoil, thus potentially affecting untilled crop root zones (Fig. 3 and *SI Appendix*, Figs. S2–S4). An important yet difficult-to-detect consequence of exceedance of the critical soil strength threshold in the subsoil is the onset of chronic compaction that negatively impacts various soil functions (9, 26). These are manifested by a persistent decline in crop yields (13, 27, 28), limited water infiltration capacity (8, 10), and a decline in other soil ecosystem services (29, 30). A key point is that the likelihood of subsoil compaction increases with increasing vehicle weights. Higher vehicle weights also limit the time windows for safe passage without the risk of root zone compaction (*SI Appendix*, Figs. S5 and S6). For illustration purposes, we have used combine harvesters to show the historical increase in vehicle weights and associated adverse consequences for soil functioning. However, similar trends of increasing weights related to efficiency gains are observed for other field operations, including in-furrow plowing, slurry spreading, and sugar beet, maize, or cotton harvesting (*SI Appendix*, section 6). Additionally, similar trends of increasing machinery weights (e.g., forwarders) and their impacts on soil are of concern in the context of forest productivity (31–33). Considerations of present mechanization levels and estimated average tractor size (linked to average farm size) reveal alarming patterns in subsoil compaction susceptibility and potential for chronic compaction in regions with intensive mechanization combined with climatic moist soil conditions (Fig. 4 and *SI Appendix*, section 7). The regions where the subsoil compaction susceptibility index (SCSI) exceeds unity agree well with global patterns of yield losses due to soil compaction presented by Sonderegger and Pfister (34). The values of the

SCSI on the global map depend on numerous assumptions regarding average tractor size, soil stress and climatic soil water content (*SI Appendix*, Figs. 13–15) that may vary locally and with conditions and timing of farming operations. The fraction of arable land that is presently at high risk of subsoil compaction is about 20% of global cropland area (Fig. 4), concentrated in mechanized regions in Europe, North America, South America, and Australia. We note that certain mechanized arid regions show considerably lower risk due to lower moisture and average higher soil strengths (e.g., western United States, southwest Australia, Saudi Arabia, and southern Russia). Conservation agriculture (35) may not necessarily alter the risk picture due to the use of heavy combines and harvesters that can induce subsoil compaction (Fig. 3 and *SI Appendix*, Fig. S11). Despite a rapid increase in the number of tractors, most of Asia (including India and China) exhibits low SCSI values due to small farms that require small tractors. Values of the SCSI are low in sub-Saharan Africa because of low mechanization levels. Nevertheless, trends in land aggregation in these regions (36) and the emergence of business models for provision of services using larger agricultural vehicles (for efficiency) may drive the SCSI toward values presently found in high-income countries.

Trends of increasing weights of agricultural machinery suggest that the focus of agricultural vehicle design on increasing efficiency, floatation, and traction may have ignored intrinsic soil limits exceeded with deeper subsoil stress propagation. Considering the narrow range of mechanical limits of most soils in temperate regions, future agricultural vehicles must be designed with intrinsic soil mechanical limits in mind to avoid chronic soil compaction. A recent trend toward using rubber track undercarriages on heavy agricultural machinery reduces contact stresses and may alleviate vertical stress in the upper subsoil, but it does not significantly reduce the risk of subsoil root zone compaction. Moreover, experimental evidence shows that adverse impacts on soil structure persist, potentially due to higher shear deformation (37) and higher loading dynamics compared with tires (38). Ironically, highly efficient tractors and harvesters may hamper progress toward increasing food production for a growing population under a changing climate (39–41) due to the unintended risk of subsoil compaction. The total weights of modern agricultural machinery exceed by far the heaviest living terrestrial animals [African bush elephants, with a maximum body mass of ca. 8,000 kg (42)] and are now approaching that of the heaviest animals that ever walked on Earth: sauropods.

The Sauropods Paradox

The similarity in mass and contact area between modern farm vehicles and sauropods raises the question: What was the mechanical impact of these prehistoric animals on land productivity? Following a similar analysis as shown for farm vehicles (Figs. 2 and 3), we hypothesize that sauropods must have compacted the subsoil during their locomotion, especially if we consider that the enormous weight of sauropods must have been supported by three feet during locomotion. The resulting mass per foot would have been 20,000 kg or more, considering the heaviest sauropod weighed 60,000 to 80,000 kg (43–45). For comparison, a modern sugar beet harvester weighs 60,000 kg when fully laden (9) but is equipped with three axles and six tires, resulting in about 10,000 kg per wheel. In other words, even the heaviest modern agricultural machinery applies only about half the weight of the heaviest sauropod per leg. We note that the difference between a sauropod footprint [the largest
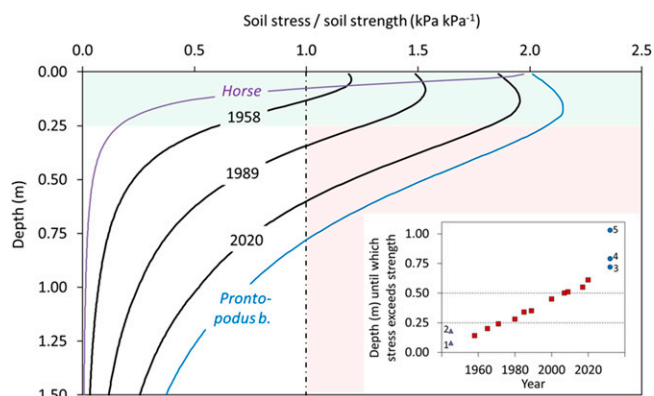
Fig. 3. Risk of soil compaction has increased over the past six decades in the course of agricultural mechanization. Soil stress is shown in relation to soil strength as a function of soil depth for typical combine harvesters of 1958, 1989, and 2020. The stress/strength profiles for a horse and a sauropod (*Prontosaurus birdi*) are shown for comparison. Soil compaction is expected for soil stress/soil strength > 1.0. The green area indicates no severe risk of compaction (above the annual tillage depth), and the red area indicates risk of permanent subsoil compaction (below the annual tillage depth). The inset shows the depth until which stress exceeds strength, indicating the progression of critical stress-exceedance depths over time (the horizontal dashed line at a 0.25-m depth indicates the typical tillage depth), for typical combine harvesters from 1958 to date (red squares), mammals (violet triangles—1, horse; 2, African elephant), and sauropods (blue circles—3, *Brachiosaurus* sp.; 4, *Prontosaurus birdi*; 5, *Argentinosaurus*).
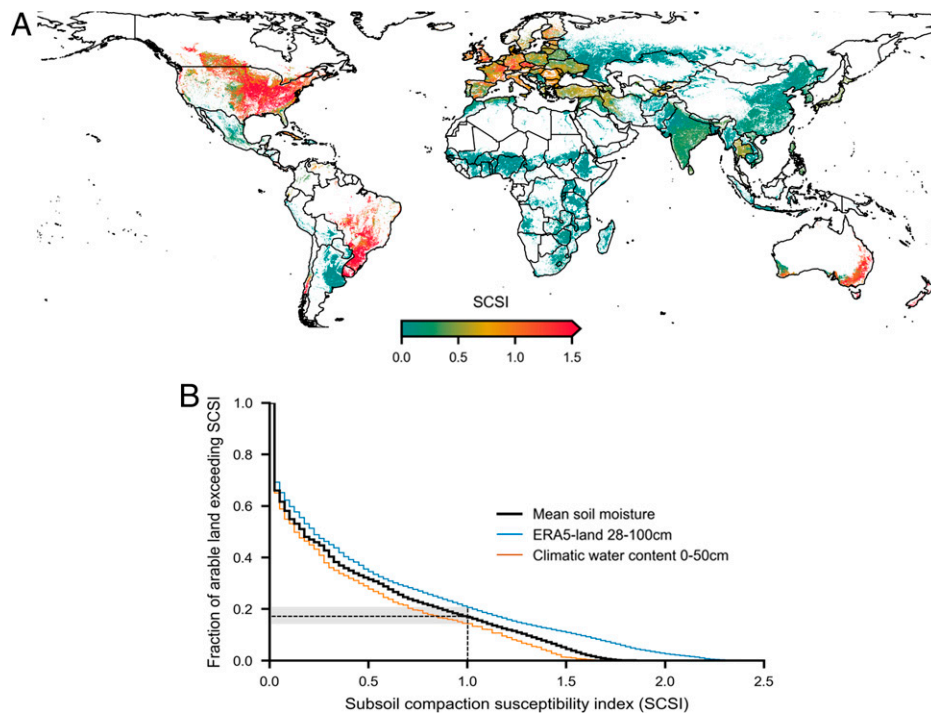
Fig. 4. Global distribution of subsoil compaction susceptibility expressed as an index relating estimated mean tractor-applied stress to soil strength at a depth of 0.5 m (SCSI). (*A*) Global map derived from mechanization levels, farm sizes, estimated tractor size, soil texture, and climatic average water content calculated at a 0.1° resolution (*SI Appendix,* section 7 for details). (*B*) Fraction of arable land exceeding a value of the SCSI, with SCSI > 1 indicating a likelihood of chronic subsoil compaction. The global fraction of arable land under threat of subsoil compaction exceeds 20% and concentrates in high-income countries with large farms and moist average soil conditions. Note the sensitivity of the calculated SCSI to the average soil moisture conditions. The ERA5-Land product (62, 63) is wetter and expands the regions under compaction risk, whereas the climatic water content procedure (60) predicts drier conditions on average, resulting in lower estimates of arable land fraction under subsoil compaction risk.

ever found is about 1.35 to 1.5 m² (45, 46)] and the footprint of a modern high-volume agricultural tire (about 1 m²; *SI Appendix,* Table S1) is less than the relative difference in mass.

The potential for significant soil compaction by foraging sauropods seems incompatible with productive land that supported renewable vegetation for feeding these prehistoric herbivores. Although the soil mechanical properties and other conditions supporting sauropods are not known, it is reasonable to assume that the soil must have received ample precipitation to support growth of vegetation, and foraging ranges explored by these giants were likely small considering the challenge of locomotion over wet soils. While resolving this paradox is beyond the scope of this study, such an intrinsic constraint must have imposed certain ecological adaptations to sustain ample vegetation and sauropod mobility, such as walking on well-compacted pathways while browsing away from the path or life partially suspended in water and foraging along the margins of water bodies [such as postulated in Smith et al. (47) concerning feeding on mangroves along ancient shorelines]. Both hypothesized strategies favor animals with long necks (44), a characteristic of sauropods that supported the successful evolution of these giants. The picture of free foraging over the landscape seems unlikely due to the risk of massive soil compaction and loss of productivity.

Conclusion

Our study provides evidence that present trends of increasing agricultural vehicle weights are not sustainable, necessitating consideration of subsoil critical stresses in future designs to supplement the present focus on traction and contact stress. Subsoil stresses induced by today's agricultural vehicles have

reached or crossed critical levels for ecological functioning of subsoil root zones, with adverse consequences for land productivity. Based on a proposed subsoil compaction susceptibility index that integrates mechanization levels and soil and climatic conditions, nearly 20% of arable land is at risk for chronic subsoil compaction in regions that are central for global food production. As the weights of modern agricultural vehicles are now approaching those of sauropods, questions regarding the potential impacts of these giants on land productivity emerge. This perplexing observation suggests constraints on the patterns of sauropod foraging behavior toward minimizing subsoil compaction risk over prehistoric landscapes to support land productivity and sauropod mobility.

Methods

Tractors. To create the global map of subsoil compaction susceptibility (Fig. 4), we used data on tractor power, mass, and typical tires from Tractorbook (*SI Appendix*, Table S4).

Soil Stress Simulations. Stress propagation in soil below agricultural tires and animal feet (Figs. 2 and 3) was modeled using the classical Boussinesq (50) solution in relation to the problem of the normal loading of the surface of a homogeneous isotropic elastic half-space. For simplicity, we assumed a circular shape for the contact area (i.e., footprint and tire–soil area) and uniform contact stress distribution across the contact area. Vertical normal stress, σ_{zz}, at depth z under the centerline of the contact area with radius a is then calculated as follows (50):

$$\sigma_{zz} = p_0 \left(1 - \frac{z^3}{\left(a^2 + z^2\right)^{3/2}} \right), \qquad [1]$$

where p_0 is the surface stress.

Assumption of a circular contact area and uniform stress distribution in the contact area results in underestimation of soil stress in the topsoil layers but has little influence on the prediction of subsurface stress (51–53), which is the focus of our analysis. In other words, the procedure applied here can be considered a conservative estimate of soil stress. Hence, our estimates of the ratio of soil stress to soil strength are also conservative.

For calculations of the SCSI (Fig. 4), we used the mean value of two vertical soil stress estimates, representing a lower and an upper soil stress estimate. As a lower soil stress estimate, we simulated vertical soil stress using uniform stress distribution at the tire–soil contact area and Eq. **1** as described above. Additionally, we considered a parabolic tire–soil contact stress distribution (51) and simulations, using a Fröhlich (54) concentration factor of 6 (20) as an upper soil stress estimate (*SI Appendix*, section 7); these simulations were performed using the SoilFlex model (55). For this, the tire–soil contact area is divided into i small elements each with an area A_i and a vertical stress $\sigma_{z,i}$ carrying the load $P_i = \sigma_{z,i} A_i$, which is treated as a point load (20). Vertical normal stress, σ_{zz}, at depth z is then calculated as follows (20):

$$\sigma_{zz} = \sum_{i=0}^{i=n} \frac{\upsilon P_i}{2\pi z_i^2} \cos^{\upsilon+2} \alpha_i, \qquad [2]$$

where α is the angle between the normal load vector and the position vector from the point load to the desired point and υ is the concentration factor (54), typically taking values between 3 and 6 (20). For $\upsilon = 3$, Eq. **2** satisfies the elastic theory of Boussinesq (50) as given in Eq. **1**.

Estimation of Soil Precompression Stress.
Soil texture. Global analysis based on SoilGrids predictions (56) reveals that loamy texture is by far the most predominant textural class in Europe, North America, and Asia (57), and we therefore used this soil textural class for estimations of soil strength (precompression stress, see below) in simulations representative of general trends, as shown in Fig. 3. We used average bulk density for loamy texture as given in Dexter (58). For calculations of the SCSI (Fig. 4), we used subsoil texture (0.3- to 0.6-m depth) from SoilGrids 2.0 (59) as detailed below.
Soil moisture. For our analysis of general trends, as shown in Fig. 3, we assumed a typical soil moisture profile for temperate climate with decreasing matric suction with depth (assuming field capacity at a 1-m depth), based on climatic soil water content (60, 61). The typical soil moisture profile corresponds to the climatic water content of central Europe (60). This was obtained from the global rainfall record of the last four decades (Multi-Source Weighted-Ensemble Precipitation database), applied to land pixels and considering internal drainage and estimates of evapotranspiration, thus providing climatic averaged soil water content. Additional simulations for other moisture profiles (both wetter and drier and again based on climatic soil water content) were performed and are shown in *SI Appendix*, section 5.

For calculations of the SCSI (Fig. 4), we averaged information from different global rainfall products to derive climatic (mean) root zone soil moisture for estimation of the soil precompression stress required for the SCSI (see below) using ERA5-Land (62, 63) and climatic water content (60, 61) as the wet and dry bounds, respectively.

Soil precompression stress. Soil precompression stress, representing the critical stress (i.e., strength) of a soil (64), was estimated from soil texture, bulk density, and soil matric suction using data and pedotransfer functions from eight studies (25, 48, 65–70) (*SI Appendix*, section 5). For Fig. 3, we used a typical soil moisture profile (see above) and presented the central value of the eight estimates of precompression stress. Estimates for either wetter or drier soil conditions, as well as information on the range of precompression stress obtained from the eight different pedotransfer functions, are given in *SI Appendix*, section 5. For calculations of the SCSI (Fig. 4), the mean value for soil precompression stress, obtained from the eight pedotransfer functions, as a function of soil moisture was applied for three different soil texture classes, as described below.

Global Distribution of Subsoil Compaction Susceptibility. The global distribution of subsoil compaction susceptibility of arable land was based on estimating soil stress induced by representative agricultural machinery, estimating typical soil strength (i.e., precompression stress), and calculating a SCSI as the ratio of soil stress to soil strength. As our focus is on subsoil, estimates of the SCSI were calculated for a 0.5-m soil depth. A flowchart of the calculations is given in *SI Appendix*, Fig. S7. Details on development of the map (Fig. 4) and the used map layers are given in *SI Appendix*, section 7, and data and maps are available at https://www.doi.org/10.5281/zenodo.6052097.

To obtain estimates of tractor-applied soil stress, we estimated for each country the distribution of tractor size from (i) global data on tractor density (Food and Agriculture Organization of the United Nations, World Bank), (ii) a mechanization-level index (ranging from 0 to 100%, with the latter indicating full mechanization) derived from the relationship between power source for field operations and tractor density (*SI Appendix*, Fig. S9), and (iii) tractor power as a function of farm size (*SI Appendix*, Fig. S8). These relationships were based on literature data at the country level (*SI Appendix*, section 7 for details). Tractor weight and wheel load were calculated from tractor power (*SI Appendix*, Table S4). Finally, soil stress was calculated from wheel load. We simulated soil stress for the most common tillage operation, i.e., conventional in-furrow plowing [ca. 80% of arable mechanized land (35, 71)], similar to in Keller et al. (11). Conventional tillage is less representative in areas of high adaption of conservation tillage (35); however, subsoil stresses of combine harvesters (with typical wheel loads twice as high as for tractors) induce similar subsoil stresses (11) (*SI Appendix*, Fig. S11). Hence, our approach using tractors, for which global data are available, is a good general indicator for subsoil stress in mechanized agriculture.

Soil precompression stress was estimated from soil texture and soil moisture using pedotransfer functions. Global distribution of subsoil texture (0.3- to 0.6-m depth) was obtained from SoilGrids 2.0 (59), and each pixel was classed into three textural classes (<15, 15 to 30, and >30% clay). We used eight different pedotransfer functions for soil precompression stress based on a literature search and used the mean of these eight estimates for each soil class as an estimate of soil strength (*SI Appendix*, sections 5 and 7). Global distribution of soil moisture was based on the mean values from two different estimates representing a dry bound [climatic water content (60)] and a wet bound [ERA5-Land (62, 63)]; *SI Appendix*, section 7, has more details.

1. R. Costanza *et al.*, Changes in the global value of ecosystem services. *Glob. Environ. Change* **26**, 152–158 (2014).
2. J. A. Foley *et al.*, Solutions for a cultivated planet. *Nature* **478**, 337–342 (2011).
3. J. Davies, The business case for soil. *Nature* **543**, 309–311 (2017).
4. A. Erktan, D. Or, S. Scheu, The physical structure of soil: Determinant and consequence of trophic interactions. *Soil Biol. Biochem.* **148**, 107876 (2021).
5. A. G. Power, Ecosystem services and agriculture: Tradeoffs and synergies. *Philos. Trans. R. Soc. Lond. B Biol. Sci.* **365**, 2959–2971 (2010).
6. E. Rabot, M. Wiesmeier, S. Schlüter, H.-J. Vogel, Soil structure as an indicator of soil functions: A review. *Geoderma* **314**, 122–137 (2018).
7. D. Or, T. Keller, W. H. Schlesinger, Natural and managed soil structure: On the fragile scaffolding for soil functioning. *Soil Tillage Res.* **208**, 104912 (2021).
8. R. Horn, H. Domżżał, A. Słowińska-Jurkiewiecz, C. van Owerkerk, Soil compaction processes and their effects on the structure of arable soils and the environment. *Soil Tillage Res.* **35**, 23–36 (1995).
9. P. Schjønning *et al.*, Driver-pressure-state-impact-response (DPSIR) analysis and risk assessment for soil compaction – A European perspective. *Adv. Agron.* **133**, 183–237 (2015).
10. A. Alaoui, M. Rogger, S. Peth, G. Blöschl, Does soil compaction increase floods? A review. *J. Hydrol. (Amst.)* **557**, 631–642 (2018).
11. T. Keller, M. Sandin, T. Colombi, R. Horn, D. Or, Historical increase in agricultural machinery weights enhanced soil stress levels and adversely affected soil functioning. *Soil Tillage Res.* **194**, 104293 (2019).
12. A. R. Graves *et al.*, The total costs of soil degradation in England and Wales. *Ecol. Econ.* **119**, 399–413 (2015).
13. T. Sonderegger, S. Pfister, S. Hellweg, Assessing impacts on the natural resource soil in life cycle assessment: Methods for compaction and water erosion. *Environ. Sci. Technol.* **54**, 6496–6507 (2020).
14. I. Håkansson, R. C. Reeder, Subsoil compaction by vehicles with high axle load extent, persistence and crop response. *Soil Tillage Res.* **29**, 277–304 (1994).
15. F. E. Berisso *et al.*, Persistent effects of subsoil compaction on pore characteristics and functions in a loamy soil. *Soil Tillage Res.* **122**, 42–51 (2012).
16. L. ten Damme *et al.*, The contribution of tyre evolution to the reduction of soil compaction risks. *Soil Tillage Res.* **194**, 104283 (2019).
17. D. H. Cumming, G. S. Cumming, Ungulate community structure and ecological processes: Body size, hoof area and trampling in African savannas. *Oecologia* **134**, 560–568 (2003).
18. F. Michilisens, P. Aerts, R. Van Damme, K. D'Août, Scaling of planar pressures in mammals. *J. Zool. (Lond.)* **279**, 236–242 (2009).
19. J. W. Wong, *Terramechanics and Off-Road Vehicle Engineering* (Elsevier Ltd, ed. 2, 2010). 10.1016/C2009-0-00403-6.
20. W. Söhne, Fundamentals of pressure distribution and soil compaction under tractor tires. *Agric. Engin.* **39**, 276–281, 290 (1958).
21. L. Alakukku *et al.*, Prevention strategies for field traffic-induced subsoil compaction: A review. Part 1. Machine/soil interactions. *Soil Tillage Res.* **73**, 145–160 (2003).
22. D. L. O. Smith, J. W. Dickson, Contributions of vehicle weight and ground pressure to soil compaction. *J. Agric. Eng. Res.* **46**, 13–29 (1990).
23. R. Horn, H. Fleige, Risk assessment of subsoil compaction for arable soils in Northwest Germany at farm scale. *Soil Tillage Res.* **102**, 201–208 (2009).
24. T. Keller *et al.*, In situ subsoil stress-strain behavior in relation to soil precompression stress. *Soil Sci.* **177**, 490–497 (2012).
25. R. Horn, H. Fleige, A method for assessing the impact of load on mechanical stability and on physical properties of soils. *Soil Tillage Res.* **73**, 89–99 (2003).
26. M. F. Nawaz, G. Bourrié, F. Trolard, Soil compaction impact and modelling. A review. *Agron. Sustain. Dev.* **33**, 291–309 (2013).
27. I. Håkansson *et al.*, Effect of high axle-load traffic on subsoil compaction and crop yield in humid regions with annual freezing. *Soil Tillage Res.* **10**, 259–268 (1988).
28. P. B. Obour, C. M. Ugarte, A meta-analysis of the impact of traffic-induced compaction on soil physical properties and grain yield. *Soil Tillage Res.* **211**, 105019 (2021).
29. W. Hu, J. Drewry, M. Beare, K. Eger, K. Muller, Compaction induced soil structural degradation affects productivity and environmental outcomes: A review and New Zealand case study. *Geoderma* **395**, 115035 (2021).
30. R. Prăvălie, Exploring the multiple land degradation pathways across the planet. *Earth Sci. Rev.* **220**, 103689 (2021).
31. M. Cambi, G. Certini, F. Neri, E. Marchi, The impact of heavy traffic on forest soils: A review. *For. Ecol. Manage.* **338**, 124–138 (2015).
32. T. Nordfjell, E. Öhman, O. Lindroos, B. Ager, The technical development of forwarders in Sweden between 1962 and 2012 and of sales between 1975 and 2017. *Int. J. For. Eng.* **30**, 1–13 (2019).
33. D. DeArmond, J. B. S. Ferraz, N. Higuchi, Natural recovery of skid trails. A review. *Can. J. For. Res.* **51**, 948–961 (2021).
34. T. Sonderegger, S. Pfister, Global assessment of agricultural productivity losses from soil compaction and water erosion. *Environ. Sci. Technol.* **55**, 12162–12171 (2021).
35. A. Kassam, T. Friedrich, R. Derpsch, Global spread of conservation agriculture. *Int. J. Environ. Stud.* **76**, 29–51 (2019).
36. N. J. Sitko, T. S. Jayne, Structural transformation or elite land capture? The growth of "emergent" farmers in Zambia. *Food Policy* **48**, 194–202 (2014).
37. R. Horn, Stress-strain effects in structured unsaturated soils on coupled mechanical and hydraulic processes. *Geoderma* **116**, 77–88 (2003).
38. M. Lamandé, M. H. Greve, P. Schjønning, Risk assessment of soil compaction in Europe – Rubber tracks or wheels on machinery. *Catena* **167**, 353–362 (2018).
39. J. P. Lynch, T. Wojciechowski, Opportunities and challenges in the subsoil: Pathways to deeper rooted crops. *J. Exp. Bot.* **66**, 2199–2210 (2015).
40. J. P. Lynch, Root phenotypes for improved nutrient capture: An underexploited opportunity for global agriculture. *New Phytol.* **223**, 548–564 (2019).
41. K. Thorup-Kristensen *et al.*, Digging deeper for agricultural resources, the value of deep rooting. *Trends Plant Sci.* **25**, 406–417 (2020).
42. O. Panagiotopoulou *et al.*, Foot pressure distributions during walking in African elephants (*Loxodonta africana*). *R. Soc. Open Sci.* **3**, 160203 (2016).
43. G. V. Mazzetta, P. Christiansen, R. A. Fariña, Giants and bizarres: Body size of some Southern American cretaceous dinosaurs. *Hist. Biol.* **16**, 71–83 (2004).
44. P. M. Sander *et al.*, Biology of the sauropod dinosaurs: The evolution of gigantism. *Biol. Rev. Camb. Philos. Soc.* **86**, 117–155 (2011).
45. R. Molina-Pérez, A. Larramendi, *Dinosaur Facts and Figures: The Sauropods and other Sauropodomorphs* (Princeton University Press, Princeton, NJ, 2020).
46. J.-D. Moreau *et al.*, Middle Jurassic tracks of sauropod dinosaurs in a deep karst cave in France. *J. Vertebr. Paleontol.* **39**, e1728286 (2019).
47. J. B. Smith *et al.*, A giant sauropod dinosaur from an Upper Cretaceous mangrove deposit in Egypt. *Science* **292**, 1704–1706 (2001).
48. M. Stettler *et al.*, Terranimo – A web-based tool for evaluating soil compaction. *Landtechn.* **69**, 132–138 (2014).
49. P. Schjønning, M. Stettler, T. Keller, P. Lassen, M. Lamandé, Predicted tyre-soil interface area and vertical stress distribution based on loading characteristics. *Soil Tillage Res.* **152**, 52–66 (2015).
50. J. Boussinesq, *Application des Potentiels à l'étude de l'équilibre et du Mouvement des Solides Élastiques* (Gauthier-Villars, Paris, 1885), p. 30.
51. E. C. Burt, R. K. Wood, A. C. Bailey, Some comparison of average to peak soil-tire contact pressures. *Trans. ASAE* **35**, 401–404 (1992).
52. K. Hammel, Soil stress distribution under lugged tires. *Soil Tillage Res.* **32**, 163–181 (1994).
53. T. Keller, J. Arvidsson, Technical solutions to reduce the risk of subsoil compaction: Effects of dual wheels, tandem wheels and tyre inflation pressure on stress propagation in soil. *Soil Tillage Res.* **79**, 191–205 (2004).
54. O. K. Fröhlich, *Druckverteilung im Baugrunde* (Springer Verlag, Wien, 1934), p. 178.
55. T. Keller, P. Défossez, P. Weisskopf, J. Arvidsson, G. Richard, SoilFlex: A model for prediction of soil stresses and soil compaction due to agricultural field traffic including a synthesis of analytical approaches. *Soil Tillage Res.* **93**, 391–411 (2007).
56. T. Hengl *et al.*, SoilGrids250m: Global gridded soil information based on machine learning. *PLoS One* **12**, e0169748 (2017).
57. C. W. Ross *et al.*, Data descriptor: HYSOGs250m, global gridded hydrological soil groups for curve-number-based runoff modeling. *Sci. Data* **5**, 150091 (2018).
58. A. R. Dexter, Soil physical quality, Part I. Theory, effects of soil texture, density, and organic matter, and effects on root growth. *Geoderma* **120**, 201–214 (2004).
59. L. Poggio *et al.*, SoilGrids 2.0: Producing soil information for the globe with quantified spatial uncertainty. *Soil (Gottingen)* **7**, 217–240 (2021).
60. S. Bickel, D. Or, Soil bacterial diversity mediated by microscale aqueous-phase processes across biomes. *Nat. Commun.* **11**, 116 (2020).
61. S. Bickel, D. Or, Dataset of global climatic soil water contents and consecutive dry days. Zenodo. https://doi.org/10.5281/zenodo.5078258 (2021). Accessed 12 February 2022.
62. J. Muñoz Sabater, ERA5-Land monthly averaged data from 1981 to present. Copernicus Climate Change Service (C3S) Climate Data Store (CDS). 10.24381/cds.68d2bb3 (2019). Accessed 3 February 2022.
63. J. Muñoz Sabater, ERA5-Land monthly averaged data from 1950 to 1980. Copernicus Climate Change Service (C3S) Climate Data Store (CDS). https://doi.org/10.24381/cds.68d2bb3 (2021). Accessed 3 February 2022.
64. J. H. Atkinson, P. L. Bransby, *The Mechanics of Soil – An Introduction to Critical State Soil Mechanics* (McGraw-Hill, London, 1978), 375 pp.
65. S. Imhoff, A. P. Silva, D. Fallow, Susceptibility to compaction, load support capacity, and soil compressibility of Hapludox. *Soil Sci. Soc. Am. J.* **68**, 17–24 (2004).
66. K. Saffih-Hdadi *et al.*, A method for predicting soil susceptibility to the compaction of surface layers as a function of water content and bulk density. *Soil Tillage Res.* **105**, 96–103 (2009).
67. P. Schjønning, M. Lamandé, Models for prediction of soil precompression stress from readily available soil properties. *Geoderma* **320**, 115–125 (2018).
68. T. Keller, M. Lamandé, P. Schjønning, A. R. Dexter, Analysis of soil compression curves from uniaxial confined compression tests. *Geoderma* **163**, 13–23 (2011).
69. J. De Pue, G. Di Emidio, A. Bezuijen, W. M. Cornelis, Functional evaluation of the various calculation methods for precompression stress. *Soil Use Manage.* **36**, 459–469 (2019).
70. E. A. S. Mendonça *et al.*, Precompression stress in response to water content and bulk density under no-till in Oxisols in southern Brazil. *Geoderma Reg.* **21**, e00261 (2020).
71. V. Porwollik, S. Rolinski, J. Heinke, C. Müller, Generating a rule-based global gridded tillage dataset. *Earth Syst. Sci. Data* **11**, 823–843 (2019).
72. C. J. Clemente, T. J. M. Dick, C. L. Glen, O. Panagiotopoulou, Biomechanical insights into the role of foot pads during locomotion in camelid species. *Sci. Rep.* **10**, 3856 (2020).
73. S. Bickel, T. Keller, D. Or, Subsoil compaction susceptibility index (SCSI). Zenodo. https://www.doi.org/10.5281/zenodo.6052097. Deposited 12 February 2022.